# A PRELIMINARY INVESTIGATION OF THE $Cr_3Si$-Mo PSEUDO-BINARY PHASE DIAGRAM

R.M. DICKERSON*, S.V. RAJ**, AND I.E. LOCCI*
*Case Western Reserve University, 10900 Euclid Ave., Cleveland, OH 44106
**NASA Lewis Research Center, 21000 Brookpark Rd., Cleveland, OH 44135

## ABSTRACT

An investigation was undertaken to study the phase relations in $Cr_3Si$ alloyed with Mo varying from 10 to 83.5 wt. % of the material. Specimens were prepared from arc-melted buttons that were subsequently heat treated at 1673 K for 200 h and air quenched to room temperature to preserve the high temperature microstructures. Alloys containing more than 20 wt. % Mo were primarily two-phase materials of $M_3Si$ and $M_5Si_3$, where M is (Cr,Mo). Three alloys contained less than 5 % of a third phase, which also had the $M_5Si_3$ crystal structure. Differential thermal analysis (DTA) was performed on several specimens at temperatures up to 2073 K in order to determine a solidus curve for the $M_3Si$ phase. Since only one DTA peak was observed in each alloy, the $M_5Si_3$ phase must melt above 2073 K, the maximum temperature examined. A preliminary pseudo-binary phase diagram for $(Cr,Mo)_3Si$ and a portion of the 1673 K isothermal section of the Cr-Mo-Si ternary phase diagram are presented.

## INTRODUCTION

Recent interest in the development of high speed civil transport (HSCT) and advanced subsonic aircraft suggests potential areas of application for intermetallic alloys with melting temperatures above 1873 K. Engine materials for these aircraft will need to endure high temperatures and stresses over longer service lives in oxidizing environments than commercial superalloys. The need for oxidation-resistant alloys suggests that Si-containing materials, which tend to form protective $SiO_2$ layers during high temperature oxidation, may be good candidates. A comparison of several silicide compounds using density, melting temperature, crystal structure, and alloyability [1] suggested that $Cr_3Si$ was worth investigating. The physical, mechanical, and oxidation properties of $Cr_3Si$, were reviewed recently [1]. Chang and Pope [2] found that $Cr_3Si$ is brittle below 1473 K, has compressive strengths varying from 175 to 450 MPa in the temperature range 1523-1673 K, and deforms on the {001}<010> slip system. In a series of studies, Anton and Shah [3-6] determined that the compressive creep stress exponent of $Cr_3Si$ changes from $\approx$ 3.4 at 1473 K to $\approx$ 2.1 at 1673 K and that the apparent activation energy for creep is approximately 500 kJ/mol. They also found better creep behavior in a Cr-39Mo-23Si (at. %) alloy, demonstrating that the addition of Mo to $Cr_3Si$ improved its high temperature mechanical properties. Oxidation studies [3] have shown $Cr_3Si$ to have properties quite similar to $MoSi_2$ at temperatures between 1273 and 1533 K. However, it has been shown [1] that $Cr_3Si$ formed mostly $Cr_2O_3$ as a surface oxide when exposed in air at 1473 and 1773 K. It was conjectured that Mo addition might improve the oxidation behavior of $Cr_3Si$-based alloys by encouraging the formation of a protective $SiO_2$ layer. Recent burner rig and cyclic and isothermal oxidation tests on several compositions of $Cr_3Si$ alloyed with Mo showed that Cr-30Mo-30Si had excellent oxidation properties [1]. Preliminary microstructural observations of the Cr-30Mo-30Si alloy revealed a microstructure consisting of 48.2% $M_3Si$, 49.2% $M_5Si_3$, and <1% $MSi_2$, where M is (Cr,Mo).

In order to optimize the compositions within the Cr-Mo-Si system, it is useful to determine the equilibrium phases expected after long term, high temperature exposure and to relate that knowledge to the macroscopic properties obtained on the alloys. The aim of the present work was to study the phase relationships in these materials as a function of composition interpolating between $Cr_3Si$ and Cr-30Mo-30Si and extrapolating on the same line toward the Mo-Si binary system.



Mat. Res. Soc. Symp. Proc. Vol. 364 © 1995 Materials Research Society

## EXPERIMENTAL

Several alloys of Cr-Mo-Si were prepared by arc-melting nominally pure element mixtures under argon. The compositions used for the present study, a subset of those being used in a larger study [8], are given in Table 1. Holding the Si content at 14.5 wt % yields stoichiometries varying from approximately $M_3Si$ in the Cr-rich alloys to nearly $M_5Si_3$ in the Mo-rich materials, thus providing an opportunity to explore the phase field between these stoichiometries. Segments of the cast buttons were heat treated in Ar at 1673 K for 200 h and air-quenched to room temperature with the intention of retaining the equilibrium phases at 1673 K for each of the alloys.

**Table 1. Sample Designations and Nominal Compositions**

| Alloy | Cr (w/o) | Mo (w/o) | Si (w/o) | Cr (a/o) | Mo (a/o) | Si (a/o) |
|---|---|---|---|---|---|---|
| 3 | 75.5 | 10.0 | 14.5 | 70.06 | 5.03 | 24.91 |
| 5 | 65.5 | 20.0 | 14.5 | 63.48 | 10.50 | 26.02 |
| 6 | 45.5 | 40.0 | 14.5 | 48.39 | 23.06 | 28.55 |
| 7 | 35.5 | 50.0 | 14.5 | 39.69 | 30.30 | 30.01 |
| 9 | 25.5 | 60.0 | 14.5 | 30.05 | 38.32 | 31.63 |
| 10 | 15.5 | 70.0 | 14.5 | 19.31 | 47.26 | 33.44 |
| 11 | 5.5 | 80.0 | 14.5 | 7.27 | 57.27 | 35.46 |
| 12 | 2.5 | 83.5 | 14.5 | 3.35 | 60.66 | 35.98 |

Polished cross-sections from each of the heat-treated samples were examined in a JEOL JSM 6100 scanning electron microscope (SEM) operating at 15 keV. A PGT IMIX (Integrated Microanalyzer for Imaging and X-Ray) system and Prism thin-window detector for x-ray energy dispersive spectrometry (XEDS) were utilized for quantitative phase area fraction and compositional analysis. Standards of Cr, and $MoSi_2$ were used for the chemical quantification. For each sample, five spectra were obtained from each phase and the overall compositions for comparison, giving very consistent results. The mean values are presented. These values have an associated 95% confidence interval of ± 2.2 at. %. Phase area fractions were determined from digitized backscattered electron (BSE) images. The phases were separable using image intensity histograms. Image analysis was performed on nine images from each alloy after one pass of a median filter to reduce noise.

Differential thermal analysis (DTA) was performed on selected alloys using a Netzsch STA 429/409 apparatus in helium with a heating and cooling rate of 600 K/h. Three heating and cooling cycles were run for each sample with a maximum temperature of 2073 K.

## RESULTS

Examples of backscattered electron (BSE) images from all eight of the alloys studied are shown in Figs. 1 and 2. The images are clustered into quartets having the same magnification. The summarized data for all the alloys given in Table 2 include nominal compositions (in at. %), measured overall compositions after heat treatment, phase area fractions, and phase compositions. The 'predicted' compositions in Table 2 are the sums of the area fractions of each phase multiplied by its composition. The greatest source of uncertainty in the predicted compositions is the area fraction determinations because the phases were not always separable in the intensity histograms when the inter-phase contrast was low, such as in Alloys 9 and 10. The lack of contrast is due to close proximity of each phase's average atomic number, which determines the intensity of the backscattered electron signal.

Alloy 3 is single phase $M_3Si$ (Fig. 1a) while Alloy 5 contains a second phase as well. (Fig. 1b). Compositional analysis (Table 2) of the second phase in alloy 5 revealed that it is $M_5Si_3$.

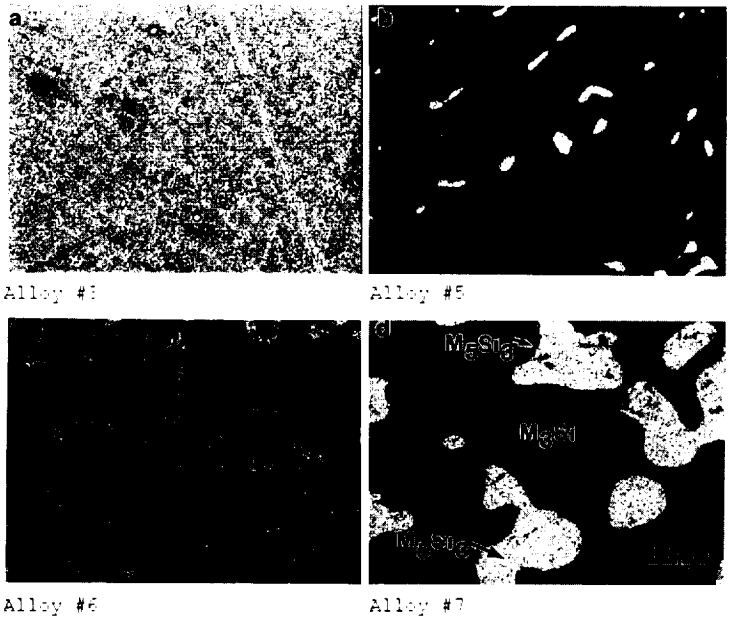


*Figure 1. Backscattered electron images of the polished sections from alloys 3,(a) 5,(b) 6,(c) and 7(d) after the 1673 K, 200 h heat treatment. All four micrographs are at the same magnification.*

The matrix of Alloy 5 is Cr-rich $M_3Si$. The microstructure of Alloy 6 is dendritic (Fig. 1(c)) and has the same phase mixture as Alloy 5. In contrast, an additional third phase is observed in Alloy 7 (Fig 1(d)), which is the alloy determined had good oxidation resistance [1]. Transmission electron microscopy and diffraction pattern analysis confirmed the SEM determinations of all three phases.

Alloys 9 and 10 are also tri-phasic (Figs. 2(a) and (b)). The interphase contrast in these materials is particularly poor because the average atomic numbers are quite close. However, pixel intensity histogram thresholding does reveal three distinct phases in both samples. The microstructures of Alloys 11 and 12 are distinctly different from the more Cr-rich alloys (Figs. 2(c) and 2(d)). $M_5Si_3$ is the majority phase in both of these samples. The $M_3Si$ phase forms as lamellae, which is most evident in Alloy 12.

X-ray energy dispersive spectrometry (XEDS) analyses of Alloys 5, 7, 9, 10, and 11 showed that a significant depletion in Cr had occurred, at least in the regions studied. Since the material has less Cr after the heat treatment, it is believed that the Cr may have evaporated while the samples were at high temperatures, either during casting or heat treatment. Alloy 6 is richer in Si and poorer in Mo than its nominal composition. This might be due to some macro-segregation of the constituents. With these effects in mind, all analyses were performed using the compositions determined experimentally and not the nominal compositions.

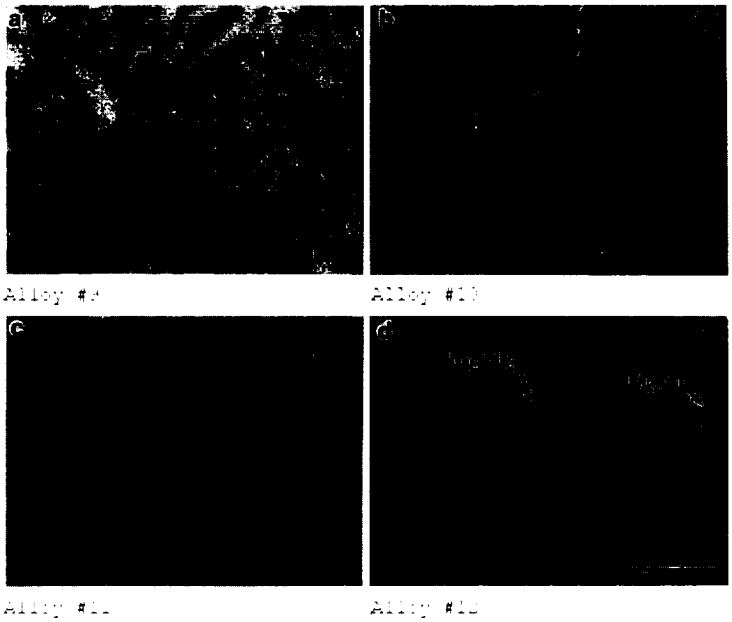

*Figure 2. Backscattered electron images of the polished sections from alloys 9(a) 10(b) 11,(c) and 12(d) after the 1673 K, 200 h heat treatment. All four micrographs are at the same magnification.*

Figure 3 shows the melting temperatures for the $M_3Si$ phase determined by DTA. The data for Alloys 5, 7, 9, and 10 are plotted. It should be noted that the melting temperatures for Alloys 11 and 12 are higher than 2073 K, the maximum temperature of the DTA apparatus. The compositions used are the XEDS-determined values for the $M_3Si$ phases, not nominal alloy compositions.

## DISCUSSION

The data presented above can be used to construct a segment of the 1673 K ternary isotherm of the Cr-Mo-Si system (Figure 4). The phase boundaries are not simple linear interpolations from the binary diagrams. The tie lines between the majority phases (filled circles) do not cross, which is consistent with thermodynamic theory. The ties to the minority $M_5Si_3$ phases in Alloys 7,9, and 10 are also shown. The compositions of the minor phases change with the overall alloy compositions and overlap the majority $M_5Si_3$ compositions. This indicates that the third phase is neither an intermediate ordered alloy nor an indicator of a stable 3-phase region at 1673 K. Therefore, the minor $M_5Si_3$ phase in alloys 7, 9 and 10 may be a remnant from a higher temperature (possibly pro-eutectic) reaction and the heat treatment times used presently are insufficient to approach the true equilibrium. Also, the tie lines in the more Cr-rich biphasic alloys are more acute than the Cr-Si elemental tie line. The tie lines must run parallel to any phase boundaries approached. This suggests that an additional region, possibly 3-phase, lies in the unexplored area defined by Alloy 5 (the most Cr-rich biphasic sample) and the $Cr_3Si$-$Cr_5Si_3$ boundary. It should also be noted that Figure 3 corresponds to the vertical isopleth of the $M_3Si$ boundary in Figure 4.

**Table 2. Sample Phase Fractions and Compositions in at. %.**

| | Area % | Hue | Si | Cr | Mo | Phase | Alloy | Area % | Hue | Si | Cr | Mo | Phase |
|---|---|---|---|---|---|---|---|---|---|---|---|---|---|
| A3 | Nominal | | 24.91 | 70.06 | 5.03 | | A9 | Nominal | | 31.63 | 30.05 | 38.32 | |
| XEDS | 100 | - | 24.06 | 70.79 | 5.15 | $M_3Si$ | | 40.44 | Bright | 39.96 | 13.38 | 46.66 | $M_5Si_3$ |
| | | | | | | | | 55.69 | Dark | 28.52 | 30.26 | 41.22 | $M_3Si$ |
| A5 | Nominal | | 26.02 | 63.48 | 10.50 | | | 3.87 | Darker | 40.23 | 21.05 | 38.72 | $M_5Si_3$ |
| | 2.74 | Bright | 43.34 | 29.52 | 27.14 | $M_5Si_3$ | Predict | | | 33.60 | 23.08 | 43.32 | |
| | 97.26 | Dark | 32.05 | 55.16 | 12.79 | $M_3Si$ | XEDS | | | 33.81 | 22.25 | 43.95 | |
| Predict | | | 32.36 | 54.46 | 13.18 | | | | | | | | |
| XEDS | | | 30.51 | 56.74 | 12.75 | | A10 | Nominal | | 33.44 | 19.31 | 47.26 | |
| | | | | | | | | 30.54 | Bright | 39.12 | 9.16 | 51.72 | $M_5Si_3$ |
| A6 | Nominal | | 28.55 | 48.39 | 23.06 | | | 67.88 | Dark | 27.42 | 20.10 | 52.47 | $M_3Si$ |
| | 14.38 | Bright | 42.13 | 24.64 | 33.24 | $M_5Si_3$ | | 1.58 | Darker | 39.70 | 17.73 | 42.57 | $M_5Si_3$ |
| | 85.62 | Dark | 31.58 | 50.47 | 17.94 | $M_3Si$ | Predict | | | 31.19 | 16.72 | 52.08 | |
| Predict | | | 33.10 | 46.76 | 20.14 | | XEDS | | | 34.88 | 13.92 | 51.20 | |
| XEDS | | | 32.10 | 48.40 | 19.50 | | | | | | | | |
| | | | | | | | A11 | Nominal | | 35.46 | 7.27 | 57.27 | |
| A7 | Nominal | | 30.01 | 39.69 | 30.30 | | | 15.72 | Bright | 25.85 | 8.77 | 65.38 | $M_3Si$ |
| | 27.76 | Bright | 41.03 | 18.15 | 40.82 | $M_5Si_3$ | | 84.28 | Dark | 38.52 | 2.87 | 58.61 | $M_5Si_3$ |
| | 4.68 | Dark | 41.18 | 22.88 | 35.95 | $M_5Si_3$ | Predict | | | 36.53 | 3.80 | 59.67 | |
| | 67.56 | Darker | 29.59 | 37.30 | 33.10 | $M_3Si$ | XEDS | | | 35.22 | 5.06 | 59.72 | |
| Predict | | | 33.31 | 31.31 | 35.38 | | | | | | | | |
| XEDS | | | 31.63 | 34.57 | 33.80 | | A12 | Nominal | | 35.98 | 3.35 | 60.66 | |
| | | | | | | | | 15.22 | Bright | 25.54 | 3.75 | 70.71 | $M_3Si$ |
| | | | | | | | | 84.78 | Dark | 38.25 | 1.51 | 60.24 | $M_5Si_3$ |
| | | | | | | | Predict | | | 36.32 | 1.85 | 61.83 | |
| | | | | | | | XEDS | | | 33.72 | 2.65 | 63.63 | |

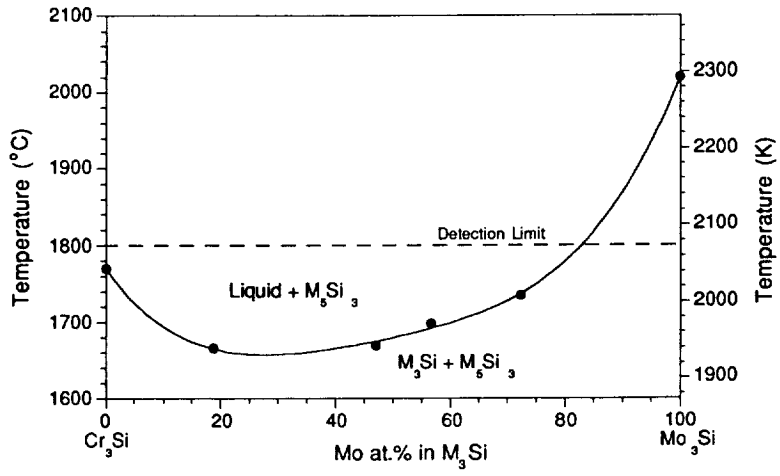


*Figure 3. Plot of the initiation of melting of the $M_3Si$ phase (solidus) curve for alloys 5, 7, 9, and 10 and binary $Cr_3Si$ and $Mo_3Si$.*

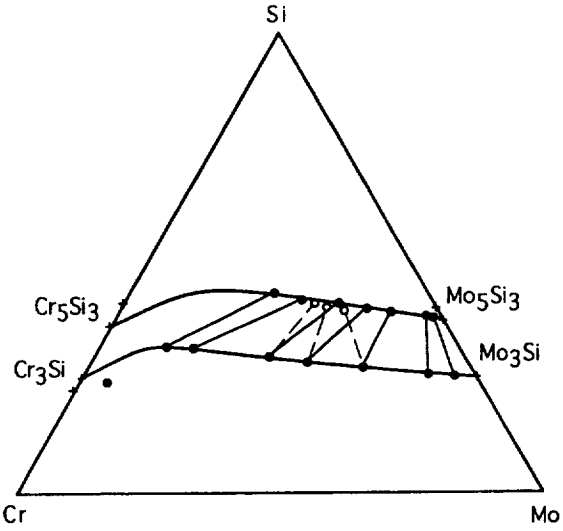


*Figure 4. Segment of the 1673 K isotherm of the Cr-Mo-Si ternary phase diagram. Filled circles connected with tie lines are the observed major phases. Open circles represent the minor $M_5Si_3$ phase in alloys 7, 9, and 10 and they are joined with a dotted line to the appropriate $M_3Si$ phase. The two-phase region boundaries are fit to the data.*

## ACKNOWLEDGMENT

The authors would like to thank Anna Palczer for performing the DTA experiments.

## REFERENCES

1. S.V. Raj, Mat. Sci. and Engr., in press.

2. C.S. Stang and D.P. Pope, in High Temperature Ordered Intermetallic Alloys IV, Vol. 213, edited by L.A. Johnson, D.P. Pope, and J.O. Stiegler (Materials Research Society, Pittsburgh, PA, 1991) p. 745.

3. D.L. Anton and D.M. Shah, in Proceedings of International Symposium on Intermatallic Compounds - Structure and Mechanical Properties (JIMIS-6), edited by O. Izumi (The Japan Institute of Metals, Sendai, Japan, 1991) p. 379.

4. D.M. Shah and D.L. Anton, Mat. Sci. and Engr., **A 153** 402 (1992).

5. D.M. Shah, D. Berczik, and D.L. Anton, Mat. Sci. and Engr., **A 155** 45 (1992).

6. D.M. Shah, in Superalloys 1992, edited by S.D. Antolvich, R.W. Strusrud, R.A. Mackay, D.L. Anton, T.Khan, R.D. Kissinger, and D.L. Klarstrom, (The Minerals, Metals, and Materials Society, Warrendale, PA, 1992) p. 409

7. E. Aitken, in Intermetallic Compounds, edited by J.H. Westbrook (Robert E. Krieger, Huntington, NY, 1977) p. 491.

8. S.V. Raj, I.E. Locci, and R.M. Dickerson (Unpublished work).